CrossMark

SN 2023emq: A Flash-ionized Ibn Supernova with Possible C III Emission

M. Pursiainen[1,2] , G. Leloudas[1] , S. Schulze[3] , P. Charalampopoulos[4] , C. R. Angus[5] , J. P. Anderson[6,7] , F. Bauer[7,8,9] ,
T.-W. Chen[10] , L. Galbany[11,12] , M. Gromadzki[13] , C. P. Gutiérrez[11,12] , C. Inserra[14] , J. Lyman[2] ,
T. E. Müller-Bravo[11] , M. Nicholl[15] , S. J. Smartt[15,16] , L. Tartaglia[17] , P. Wiseman[18] , and D. R. Young[15]

[1] DTU Space, National Space Institute, Technical University of Denmark, Elektrovej 327, DK-2800 Kgs. Lyngby, Denmark
[2] Department of Physics, University of Warwick, Gibbet Hill Road, Coventry, CV4 7AL, UK
[3] The Oskar Klein Centre, Department of Physics, Stockholm University, AlbaNova, SE-10691 Stockholm, Sweden
[4] Department of Physics and Astronomy, University of Turku, FI-20014 Turku, Finland
[5] DARK, Niels Bohr Institute, University of Copenhagen, Copenhagen, Denmark
[6] European Southern Observatory, Alonso de Córdova 3107, Casilla 19, Santiago, Chile
[7] Millennium Institute of Astrophysics MAS, Nuncio Monsenor Sotero Sanz 100, Off. 104, Providencia, Santiago, Chile
[8] Instituto de Astrofísica, Facultad de Física, Pontificia Universidad Católica de Chile, Campus San Joaquín, Av. Vicuña Mackenna 4860, Macul Santiago, 7820436,
Chile
[9] Centro de Astroingeniería, Facultad de Física, Pontificia Universidad Católica de Chile, Campus San Joaquín, Av. Vicuña Mackenna 4860, Macul Santiago,
7820436, Chile
[10] Technische Universität München, TUM School of Natural Sciences, Physik-Department, James-Franck-Straße 1, D-85748 Garching, Germany
[11] Institute of Space Sciences (ICE, CSIC), Campus UAB, Carrer de Can Magrans, s/n, E-08193 Barcelona, Spain
[12] Institut d'Estudis Espacials de Catalunya (IEEC), Gran Capità, 2-4, Edifici Nexus, Desp. 201, E-08034 Barcelona, Spain
[13] Astronomical Observatory, University of Warsaw, Al. Ujazdowskie 4, 00-478 Warszawa, Poland
[14] Cardiff Hub for Astrophysics Research and Technology, School of Physics & Astronomy, Cardiff University, Queens Buildings, The Parade, Cardiff, CF24
3AA, UK
[15] Astrophysics Research Centre, School of Mathematics and Physics, Queens University Belfast, Belfast, BT7 1NN, UK
[16] Department of Physics, University of Oxford, Keble Road, Oxford, OX1 3RH, UK
[17] INAF—Osservatorio Astronomico d'Abruzzo, via M. Maggini snc, I-64100 Teramo, Italy
[18] School of Physics and Astronomy, University of Southampton, Southampton, SO17 1BJ, UK

Abstract

SN 2023emq is a fast-evolving transient initially classified as a rare Type Icn supernova (SN), interacting with a H- and He-free circumstellar medium (CSM) around maximum light. Subsequent spectroscopy revealed the unambiguous emergence of narrow He lines, confidently placing SN 2023emq in the more common Type Ibn class. Photometrically, SN 2023emq has several uncommon properties regardless of its class, including its extreme initial decay (faster than >90% of Type Ibn/Icn SNe) and sharp transition in the decline rate from 0.20 to 0.07 mag day^{-1} at +20 days. The bolometric light curve can be modeled as CSM interaction with $0.32 M_\odot$ of ejecta and $0.12 M_\odot$ of CSM, with $0.006 M_\odot$ of nickel, as expected of fast, interacting SNe. Furthermore, broadband polarimetry at +8.7 days ($P = 0.55\% \pm 0.30\%$) is consistent with spherical symmetry. A discovery of a transitional Type Icn/Ibn SN would be unprecedented and would give valuable insights into the nature of mass loss suffered by the progenitor just before death, but we favor an interpretation that SN 2023emq is a Type Ibn SN that exhibited flash-ionized features in the earliest spectrum, as the features are not an exact match with other Type Icn SNe to date. However, the feature at 5700 Å, in the region of C III and N II emission, is significantly stronger in SN 2023emq than in the few other flash-ionized Type Ibn SNe, and if it is related to C III, it possibly implies a continuum of properties between the two classes.

Unified Astronomy Thesaurus concepts: Supernovae (1668)

Supporting material: machine-readable table

1. Introduction

The study of stellar explosions entered a new era in the wake of untargeted, high-cadence transient surveys allowing the discovery of transient phenomena that evolve on much faster timescales than typically expected of supernovae (SNe). Such rapidly evolving transients (RETs) were first discovered in archival searches in surveys such as Pan-STARRS1 Medium Deep Survey (Drout et al. 2014) and Dark Energy Survey (Pursiainen et al. 2018; Wiseman et al. 2020), resulting in large samples of spectroscopically unclassified events. Even without classifications these events expanded our understanding of

stellar deaths as their light curves evolved too fast to be explained by the decay of radioactive ^{56}Ni—the canonical power source of many typical SNe—and alternative power sources had to be considered.

In recent years an increasing number of fast events have been discovered in real time allowing intense follow-up campaigns. A significant number of them appear to be interacting H-poor SNe (e.g., Ho et al. 2023), either Type Ibn SNe characterized by a plethora of narrow helium emission lines (e.g., Foley et al. 2007; Pastorello et al. 2008), or Type Icn SNe with emission lines of carbon and oxygen (e.g., Gal-Yam et al. 2022; Perley et al. 2022). While tens of Type Ibn SNe have been discovered over the last 15 yr, so far only five Type Icn SNe have been identified—all within the past 4 years. These are SN 2019hgp (Gal-Yam et al. 2022), SN 2019jc (Pellegrino et al. 2022a), SN 2021csp (Fraser et al. 2021; Perley et al. 2022), SN 2021ckj

(Pellegrino et al. 2022a; Nagao et al. 2023), and SN 2022ann (Davis et al. 2023). Although not all Type Ibn SNe are considered to be fast evolving (e.g., Inserra 2019), a significant subpopulation of them evolve on similar timescales to RETs, while all Type Icn SNe fall into this bright-and-fast parameter space.

The existence of transitional events that change type between Type Ibn and IIn SNe over time (e.g., Pastorello et al. 2015a; Reguitti et al. 2022), suggests a continuum in the circumstellar material (CSM) properties of these events and consequently in the mass-loss history of their progenitor stars. It may therefore be reasonable to expect that transitional events between non-hydrogen-dominated CSM events (i.e., Type Icn to Ibn) also exist, although such events have not been identified to date. The discovery of such potential transitional events would be extremely valuable for our understanding of how massive stars lose their mass and create their CSM during their final stages giving insight into the chemical structure of the progenitor and the continuous or episodic nature of their mass loss.

Here we present an analysis of SN 2023emq, an SN initially identified as a Type Icn SN (Pellegrino et al. 2023), but which evolved to resemble a Type Ibn SN $\sim$10 days later (Pursiainen & Leloudas 2023), possibly implying transitional nature. This Letter is structured as follows: in Section 2 we present the observations and the data reduction procedures, in Section 3 we present the analysis of the data, and in Section 4 we conclude our findings. The spectroscopy and photometry presented in this Letter have been corrected for Milky Way extinction $E_{B-V} = 0.105$ (Schlafly & Finkbeiner 2011). Throughout the Letter, we assume a flat ΛCDM cosmology with $\Omega_M = 0.3$ and $H_0 = 70 \, \mathrm{km \, s^{-1} \, Mpc^{-1}}$ and adopt redshift $z = 0.0338$.

2. Observations and Data Reduction

SN 2023emq was discovered by Asteroid Terrestrial-impact Last Alert System (ATLAS; Tonry et al. 2018; Smith et al. 2020) on 2023 April 1 under the name ATLAS23ftq, with a previous nondetection 2 days prior (Tonry et al. 2023). The SN is associated with LEDA797708 (Makarov et al. 2014), a visibly blue galaxy in Pan-STARRS1 3π images, with an offset of $\sim3\farcs7$ from the brightest core region (Flewelling et al. 2020). A late-time image of the environment obtained with FOcal Reducer and low dispersion Spectrograph (FORS2; Appenzeller et al. 1998) on the Very Large Telescope (VLT) at European Southern Observatory (ESO), Paranal, Chile, is shown in Figure 1.

The photometry of SN 2023emq was collected from the public ATLAS and Zwicky Transient Facility (ZTF; Bellm et al. 2019) surveys, and with target-of-opportunity observations with the Neil Gehrels Swift Observatory UV-Optical telescope (UVOT; PIs: Brown and Pellegrino). The late-time ($\gtrsim$+20 days) evolution was monitored with aperture photometry from Alhambra Faint Object Spectrograph and Camera (ALFOSC) mounted on the Nordic Optical Telescope at La Palma, Spain (PI: Pursiainen) and from FORS2/VLT with a Director's Discretionary Time (DDT) Programme (2111.D-5006; PI: Pursiainen). The ATLAS o- and c-band light curves were generated using the ATLAS Forced Photometry service[19] (Shingles et al. 2021). The ZTF g- and r-band light curves were collected using the Alerce (Förster et al. 2021) and Lasair

---

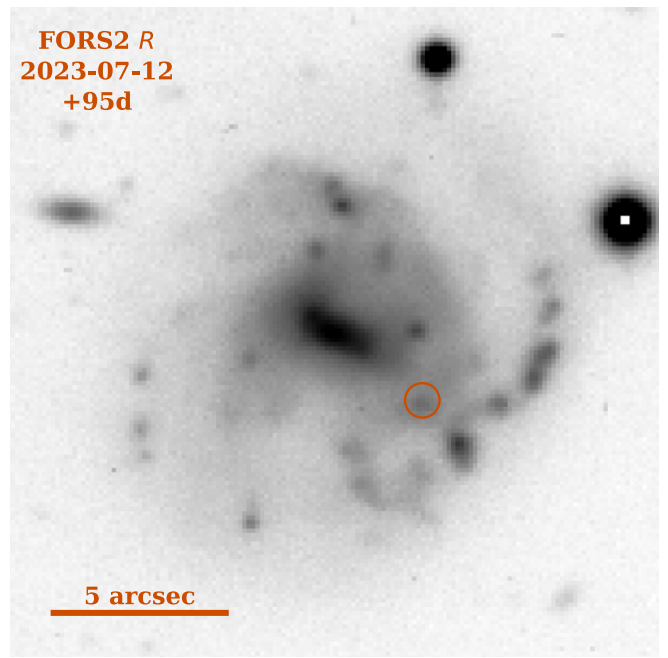[19] https://fallingstar-data.com/forcedphot/

Figure 1. The host environment of SN 2023emq in the VLT/FORS2 R-band observation taken at +95 days (2023 July 12) when the SN was already undetectable (see Table 1). The location of the SN (red circle) is on top of a bright region of the host galaxy.

(Smith et al. 2019) brokers. The light curves from Swift UVOT were reduced following Charalampopoulos et al. (2023). The photometric data are provided in Table 1.

The spectra of SN 2023emq were obtained with NOT/ALFOSC, ESO Faint Object Spectrograph and Camera 2 (EFOSC2) on the New Technology Telescope (NTT) at La Silla observatory, Chile by the extended Public ESO Spectroscopic Survey for Transient Objects plus (ePESSTO+; Smartt et al. 2015) survey and VLT/X-Shooter (Vernet et al. 2011) under the DDT program. The NOT spectrum was reduced using the PyNOT-redux reduction pipeline,[20] the NTT spectrum with the PESSTO pipeline (Smartt et al. 2015), and the X-Shooter spectrum as described in Selsing et al. (2019). We also analyzed the Global SN Project classification spectrum (Pellegrino et al. 2023) available in WISeREP[21] (Yaron & Gal-Yam 2012). The spectral log is provided in Table 2. Finally, we obtained one epoch of NOT/ALFOSC V-band imaging polarimetry on 2023 April 14 (+8.7 days). The data were reduced following Pursiainen et al. (2023).

3. Analysis

3.1. Photometry

The multiband light curve of SN 2023emq is shown in Figure 2 (top). While the decline is well covered, only the ATLAS o-band has prepeak data. To estimate the peak MJD and magnitude we use Gaussian process (GP) interpolation using the setup presented in Pursiainen et al. (2020) and find the peak to be at MJD $\sim$ 60040 and -18.7 ± 0.1 mag. To highlight the extreme evolution timescale of SN 2023emq, we compare its light curve to the enigmatic AT 2018cow and to example Type Icn/Ibn SNe chosen for their fast light curve

---

[20] https://github.com/jkrogager/PyNOT/
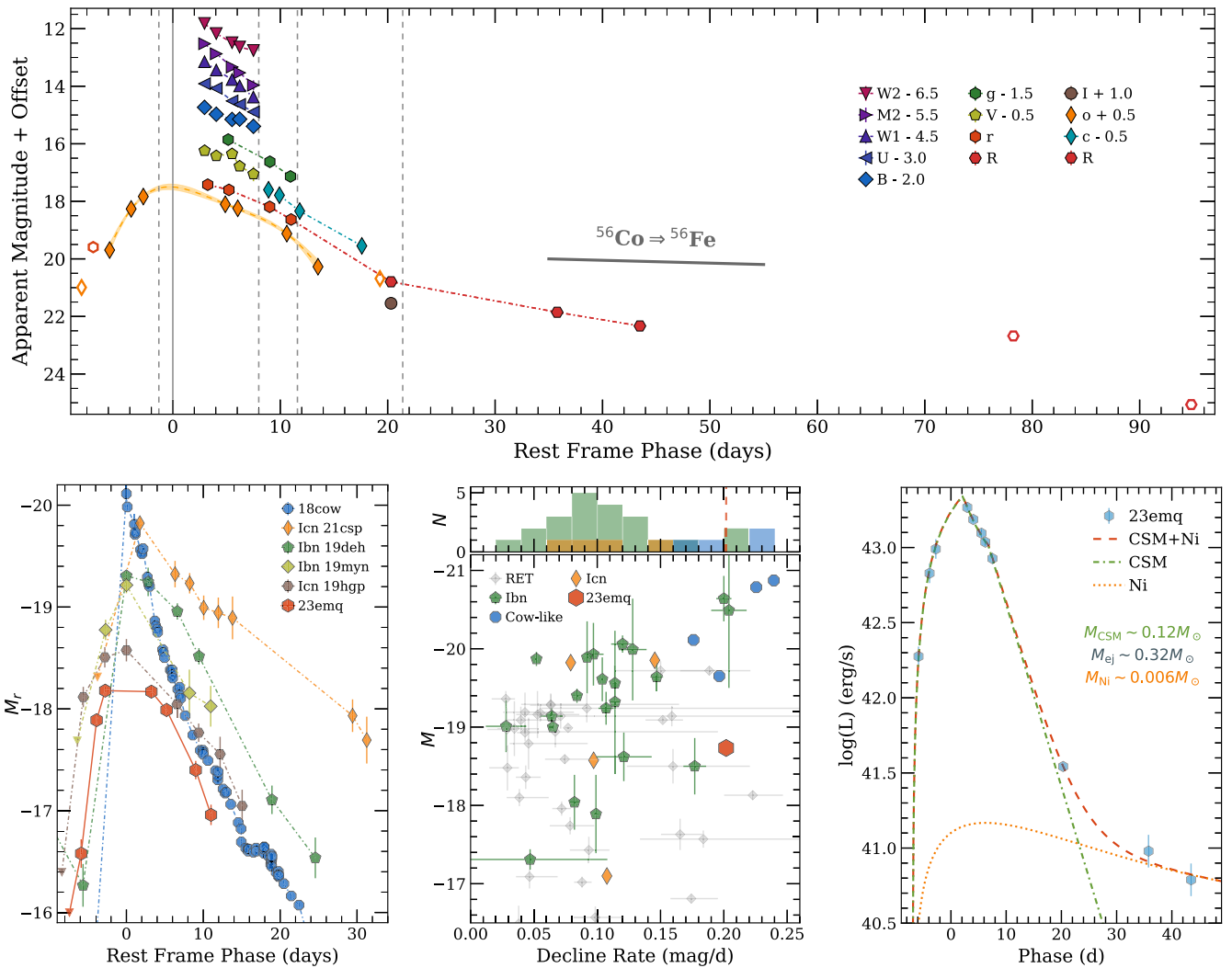[21] https://www.wiserep.org

Figure 2. Photometric qualities of SN 2023emq. Top: the multiband light curve of SN 2023emq. Open markers refer to nondetections (5σ). The spectral epochs are highlighted with dashed lines. The interpolated o-band GP light curve is shown over the data, and the decline rate of ^{56}Co is drawn for comparison. The late-time decline rate is significantly faster than the ^{56}Co rate, and the decline continued fast until the SN was no longer detected at +78 and +95 days. Bottom left: the ATLAS o-band light curve of SN 2023emq in comparison to r-band light curves of example fast events. The light curves are collected from ZTF via the Alerce broker (Förster et al. 2021) except for AT 2018cow, where data presented in Prentice et al. (2018) and Perley et al. (2019) were used. Bottom middle: absolute magnitude vs. decline rate of fast-evolving transients. Values of Type Icn SNe (Pellegrino et al. 2022a), cow-like transients (Prentice et al. 2018; Perley et al. 2019, 2021; Ho et al. 2020; Yao et al. 2022), and SN 2023emq were obtained by fitting the first 20 days of postpeak r-band light curves linearly. The values for RETs are taken from Pursiainen et al. (2018), and the used bands (g, r, i, or z) were chosen to be the closest to the rest-frame r band. Type Ibn SNe are collected from Hosseinzadeh et al. (2017), where data are presented mostly in the R band. On the top histogram we show the number (N) of transients per decline rate with SN 2023emq highlighted with a dashed red line. No Type Icn SNe and only 2/22 Type Ibn SNe are faster than SN 2023emq. Bottom right: the best-fitting combined CSM and nickel decay model (Chatzopoulos et al. 2012, 2013) to the bolometric light curve of SN 2023emq. The derived CSM and ejecta masses are similar, but smaller in comparison to other Type Ibn/Icn SNe as expected given the fast light-curve evolution near peak. The nickel mass is comparable to fast-evolving Type Ibn/Icn SNe.

evolution in Figure 2 (left). While the rise of the SN is not exceptional, its initial decline is fast regardless of its type, and by the time of the last spectrum at ∼+20 days, the SN had already declined by 3.5 mag in brightness. In fact, the decline rate in the first 15 days postpeak (∼0.20 mag day^{-1}) is at the extreme end of Type Ibn/Icn SNe and comparable to the events similar to AT 2018cow (e.g., Prentice et al. 2018; Perley et al. 2019, 2021; Ho et al. 2020; Yao et al. 2022), as demonstrated in Figure 2 (middle). However, based on our NOT R-band data we can determine that after the observation at +20 days the decline slowed to 0.07 mag day^{-1}—3 times slower than the early decline. While the decline rates of Type Ibn SNe are expected to decrease in time and similar breaks have been seen before (e.g., SN 2015G; Shivvers et al. 2017), such extreme

transitions are rare in the population (see, e.g., Hosseinzadeh et al. 2017). Out of the Type Icn SNe, only SN 2022ann has exhibited a similar transition where the decline rate decreased from a maximum of ∼0.14 to ∼0.03 mag day^{-1} (Davis et al. 2023).

The late-time decline of SN 2023emq is faster than that expected from the ^{56}Co to ^{56}Fe decay (0.0098 mag day^{-1}), but the decay likely contributes at these epochs. Using the semianalytical light-curve models of Chatzopoulos et al. (2012, 2013), we fit the bolometric light curve of SN 2023emq (for details see Appendix A) with a combined CSM interaction and nickel decay model. We assumed shell-like CSM with a setup presented by Pellegrino et al. (2022a) for Type Icn SNe except for the opacity for which we used $\kappa = 0.2$ cm^2 s^{-1} as
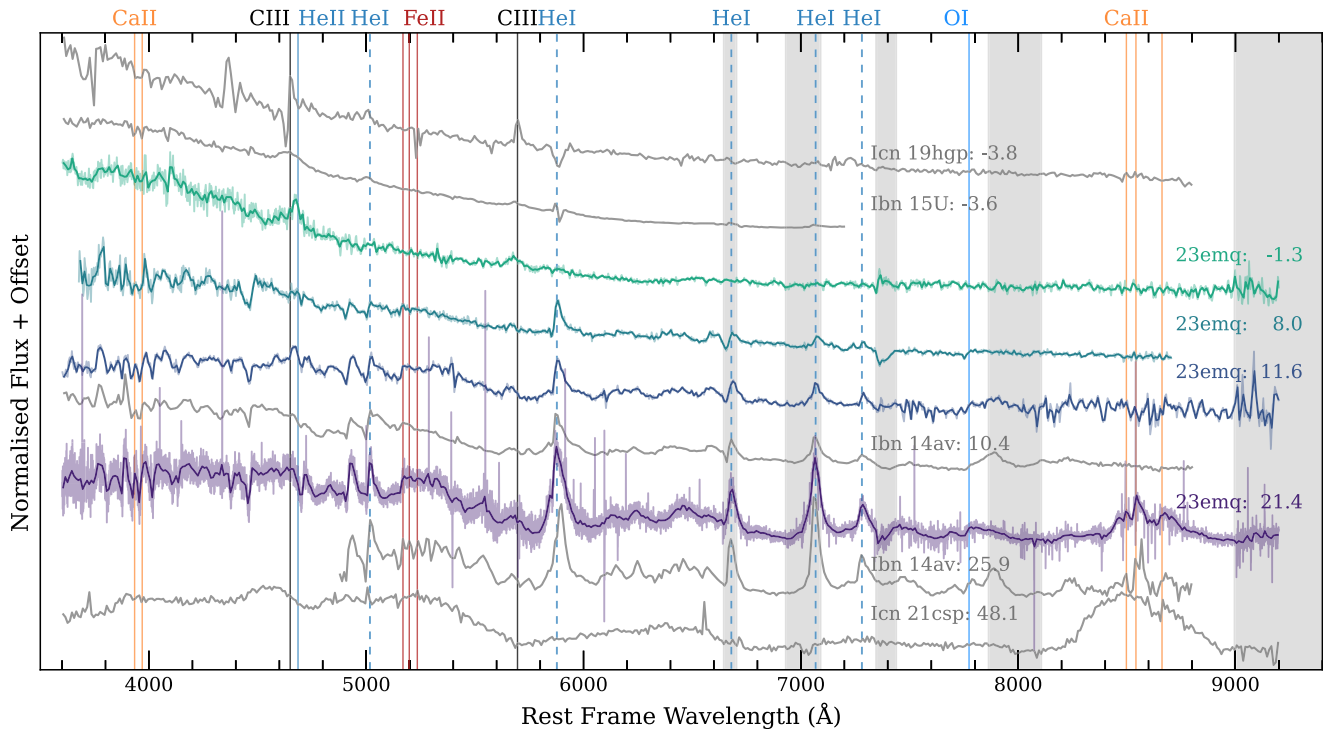
Figure 3. The spectroscopic time series of SN 2023emq (in colors) in comparison to the Type Icn SNe 2019hgp (Gal-Yam et al. 2022) and 2021csp (Perley et al. 2022) and the Type Ibn SNe 2015U (Shivvers et al. 2016) and 2014av (Pastorello et al. 2016) in gray. Spectral epochs are presented with respect to peak brightness. The first spectrum resembles that of SN 2015U, and the latest spectrum is virtually identical to SN 2014av. As already noted by Perley et al. (2022), the continuum emission of SN 2021csp at late times is very similar to the continuum seen in Type Ibn SNe including SN 2023emq. The most prominent He I features are marked with dashed lines, other strong features with solid lines, and tellurics are shown in gray bands. Note that the spectrum of the highly reddened SN 2015U is artificially dereddened for visual comparison.

appropriate for H-poor CSM (Chatzopoulos et al. 2013). As shown in Figure 2 (right), we find a good fit with $M_{\rm CSM} = 0.12^{+0.01}_{-0.01} M_{\odot}$ and $M_{\rm ejecta} = 0.32^{+0.04}_{-0.04} M_{\odot}$ (1σ) with $M_{\rm Ni} = 0.006^{+0.001}_{-0.001} M_{\odot}$. The recovered values of $M_{\rm CSM}$ and $M_{\rm ejecta}$ are smaller than found in the literature for Type Ibn SNe (e.g., Pellegrino et al. 2022b), as expected given the fast photometric evolution. The $M_{\rm Ni}$ is similar to the lowest estimates for Type Ibn/Icn SNe (e.g., Pellegrino et al. 2022a). However, based on our late-time nondetections the decline continued furiously. The SN was no longer detected in host-subtracted NOT R-band photometry taken at +78 days with a 5σ upper limit of 22.7 mag. A deeper limit of 25.1 mag was obtained at +95 days with VLT. As the decline continued faster than expected of ^{56}Co decay, the amount of ^{56}Ni synthesized in the explosion has to be truly marginal.

3.2. Spectroscopy

The spectral time series of SN 2023emq is compared to example Type Ibn and Icn SNe, chosen based on their spectral similarity to SN 2023emq, in Figure 3. We adopt a redshift of $z = 0.0338$, determined based on host-galaxy emission lines present in the 2D X-Shooter spectrum. In the classification spectrum, the most notable emission lines at 5700 Å and 4690 Å are identified as C III λ5696 and a blend of C III λ4650 and He II λ4686 (Pellegrino et al. 2023). These lines are common in Type Icn SNe, as demonstrated by well-studied SN 2019hgp (Gal-Yam et al. 2022), but emission at similar wavelengths has also been seen in a few Type Ibn SNe (e.g., SN 2015U). In the subsequent spectra the SN has evolved into a typical Type Ibn SN characterized by strong He I emission

lines. The spectra are virtually identical to that of Type Ibn SN 2014av shown in the figure.

The spectral evolution of the SN suggests that it could be a transitional Type Icn/Ibn SN, but the question relies on whether the early spectroscopic signatures are also seen in Type Ibn SNe, and important SNe to compare SN 2023emq to are the flash-ionized Type Ibn SNe 2010al (Pastorello et al. 2015a), 2019uo (Gangopadhyay et al. 2019), and 2019wep (Gangopadhyay et al. 2022). SNe often exhibit short-lived flash-ionized features early in their evolution as a result of ionization of the nearby CSM by the supernova shock breakout (e.g., Gal-Yam et al. 2014). All three SNe exhibit a strong emission feature at 4650 Å due to a blend of N III, C III, and He II, as is typical for flash-ionized spectra of young SNe (see, e.g., Khazov et al. 2016; Bruch et al. 2021, 2023). However, while no emission is present at 5700 Å in SN 2010al, in SN 2019uo and SN 2019wep extremely faint C III λ5696 emission is reported. This is also the case for H-rich flash-ionized spectra, as the line is typically extremely faint if seen at all (e.g., SN 1998S; Fassia et al. 2001). Furthermore, Shivvers et al. (2016) showed that a similar but stronger emission line at 5700 Å was also seen in an early spectrum of Type Ibn SN 2015U in addition to the blended emission line at 4650 Å (see Figure 3). The authors suggested that the line is N II λ5680, supported by the presence of several N II absorption lines in the later spectra (Pastorello et al. 2015b; Shivvers et al. 2016). Regardless of the exact identification of the line in SN 2023emq, emission has been detected at the two wavelengths in both Type Ibn and Icn SNe, and the presence of emission alone does not warrant a Type Icn classification.
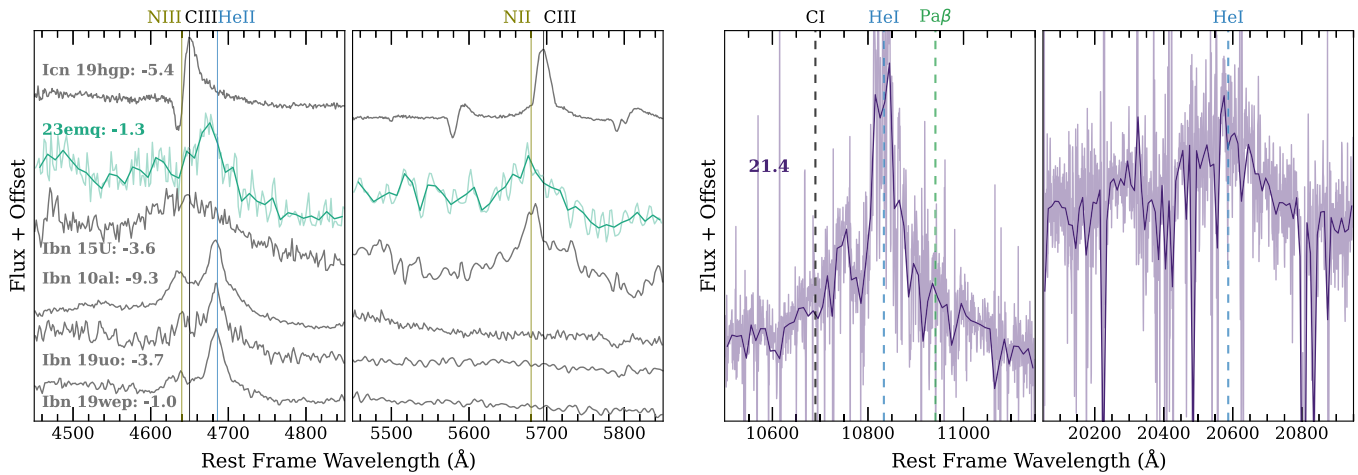
Figure 4. Left: the classification spectrum of SN 2023emq with the possible line identifications. The feature at 4690 Å is dominated by He II λ4686 with faint blue excess possibly caused by either N III λ4640 or C III λ4650. At 5700 Å the emission could be either N II λ5680 or C III λ5696. The spectrum of SN 2015U from Figure 3 as well as early spectra of the Type Icn SN 2019hgp (Gal-Yam et al. 2022) and the flash-ionized Type Ibn SNe 2010al, 2019uo, and 2019wep (Pastorello et al. 2015a; Gangopadhyay et al. 2019, 2022) are shown for comparison. Emission is seen in all SNe around 4650 Å. At 5700 Å the emission feature is either faint (SN 2015U) or not clearly detected (SNe 2010al, 2019uo, 2019wep) in the Type Ibn SNe, but it is prominent in the Type Icn SN 2019hgp. Right: the only notable features in the X-Shooter NIR spectrum. He I λ10830 is clear, but the strong C I emission line λ10690 seen in Type Icn SN 2021csp (Fraser et al. 2021) is not present. He I λ20587 is also tentatively identified.
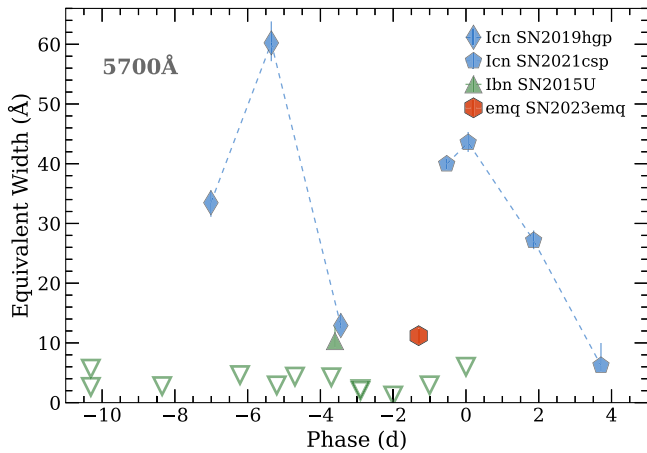
Figure 5. Equivalent width (EW) of the emission at 5700 Å as function of rest-frame phase for SN 2023emq, Type Icn SNe 2019hgp and 2021csp, and flash-ionized Type Ibn SNe. For Type Ibn SNe, the emission feature is clearly seen in only SN 2015U (see Figure 4), and for the other Type Ibn spectra we show 3σ upper limits (open triangles) determined assuming a Gaussian profile with FWHM measured for SN 2023emq ($\sim$3000 km s^{-1}). SN 2023emq does not exhibit as prominent emission as seen in most Type Icn spectra, but the line is also far more significant than seen in most flash-ionized Type Ibn SNe, possibly implying a continuum of properties between the two classes. The EWs were estimated with Gaussian fits over a linear background. For Type Ibn SNe we used the spectra of SN 2010al, SN 2015U, SN 2019uo, and SN 2019wep that exhibited the strong blended emission at 4650 Å—indicative of the flash-ionized phase. For the Type Icn SN 2019hgp and SN 2021csp we used the spectra that showed C III λ5696 emission, excluding the lower-resolution LT/SPRAT spectra (for details see Gal-Yam et al. 2022; Perley et al. 2022).

In Figure 4 (left), we investigate what emission lines are present in the first spectrum in comparison to Type Ibn and Icn SNe. The line that best matches the feature at 4690 Å is He II, with a fainter contribution from N III/C III on the blue side of the feature. The presence of He II is indicative of Type Ibn SN, as in Type Icn the line is not prominent (e.g., Pellegrino et al. 2022a). Furthermore, the feature of Type Ibn SN 2015U appears to have the same shape as in SN 2023emq if the He II contribution is ignored, while in Type Icn SNe C III λ4650

typically shows a P Cygni profile not seen in SN 2023emq. At 5700 Å the line is well matched with both C III λ5696 and N II at 5680 Å and cannot be clearly distinguished. In comparison to Type Ibn SNe, only SN 2015U exhibits any clear emission in the interval, and in this regard SN 2023emq appears more similar to Type Icn SNe, where the emission is prominent. The trend is also visible in Figure 5 where we show the equivalent widths (EWs) of emission at 5700 Å for early spectra of Type Icn SNe 2019hgp and 2021csp and the flash-ionized Type Ibn SNe against SN 2023emq. The EW of SN 2023emq ($11.2^{+1.2}_{-1.1}$ Å) is smaller than in most of the Type Icn spectra, but comparable to the ones measured at later phases just before C III emission faded away (e.g., Perley et al. 2022). On the other hand, SN 2023emq is similar to SN 2015U, but clearly above the 3σ upper limits (open triangles) estimated for the other Type Ibn SNe.

Finally, we searched the later spectra of SN 2023emq for signatures of C II or C I as seen in Type Icn SNe, but found no clear features. In the X-Shooter near-infrared (NIR) spectrum, taken at +21.4 days, we identify a clear He I λ10830 emission line (Figure 4, right), but do not see the strong C I λ10690, detected in Type Icn SN 2021csp at a similar epoch (+20.5 days; Fraser et al. 2021).

Given the presence of the prominent He II emission in the first spectrum, the early spectral similarity to SN 2015U and the flash-ionized Type Ibn SNe as well as the unambiguous Type Ibn nature after peak brightness, we favor the interpretation that SN 2023emq is a flash-ionized Type Ibn SN. The unusually prominent emission line at 5700 Å might imply some kind of continuum between Type Icn and Ibn SNe and could indicate that the SN 2023emq is between the two populations if it is related to C III. However, due to the unclear nature of the line, it is possible that it is related to N II like suggested for SN 2015U (Shivvers et al. 2016). In this case, SN 2023emq is the second example of a Type Ibn SN with N II emission with no obvious connection to Type Icn SNe.

We also used the X-Shooter spectrum to investigate the effect of host-galaxy extinction. The Na I D doublet, which is typically used to estimate extinction in a galaxy, is not clearly
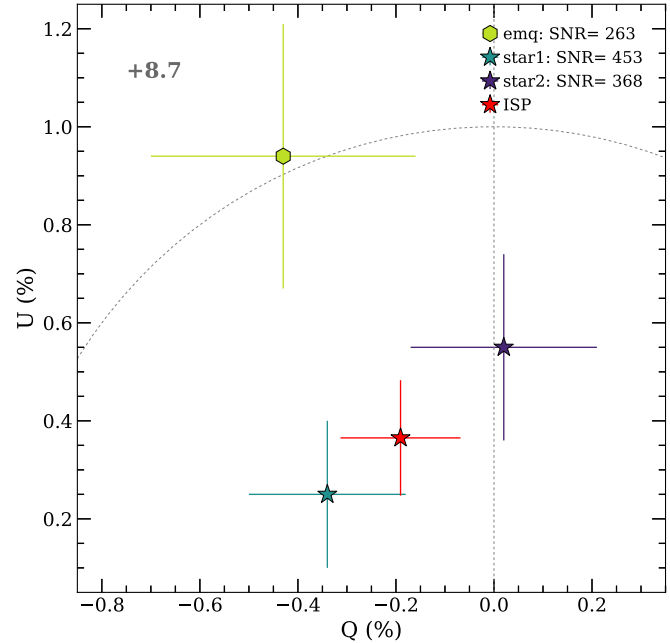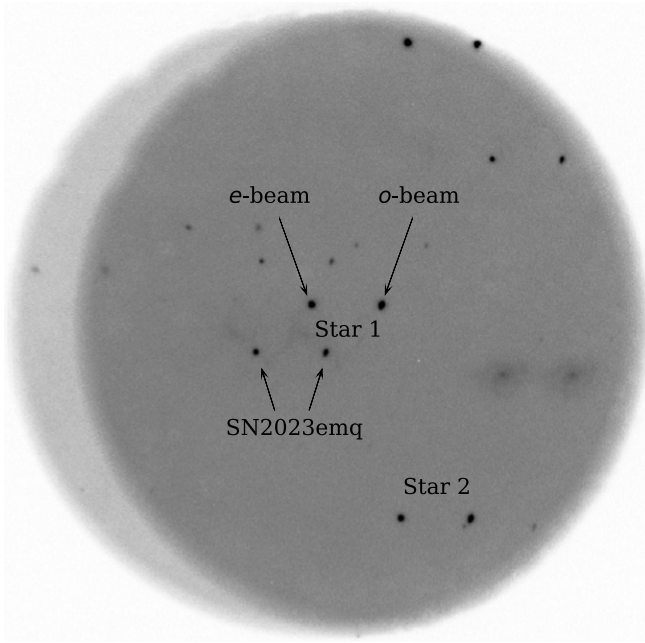
Figure 6. The NOT *V*-band polarimetry of SN 2023emq taken at +8.7 days postpeak. Left: the field of view of the observation. In the polarimetric mode, the extraordinary (*e*) and ordinary (*o*) beams are overlaid 15″ apart. The SN and the two bright stars are marked. Other sources in the image were either too faint or too close to the edge for reliable estimation of the Stokes parameters. Right: the Stokes *Q*–*U* plane. Both the SN and the two stars found in the image are shown. The SN is clearly offset from the stars. After correcting for the Galactic ISP and polarization bias, we find intrinsic polarization of $P = 0.55\% \pm 0.30\%$. The dashed lines mark the location of $Q = 0\%$ and $P = 1\%$.

visible in our high-resolution X-Shooter spectrum, and we can estimate the upper limit for E_{B-V} of the host by generating Gaussian absorption profiles over the spectrum. Assuming that the FWHM of the line is the resolution of the spectrograph (35 km s^{-1} at 5890 Å), we find a 3σ limit for the total equivalent width of the doublet is EW ~ 0.146 Å. Using the empirical equation of Poznanski et al. (2012), this equates to $E_{B-V} \lesssim 0.02$, indicating that the effect of the host-galaxy extinction should be negligible.

3.3. Polarimetry

The polarimetry taken at +8.7 days shows that SN 2023emq is polarized as demonstrated in Figure 6 (right). We measure the dimensionless Stokes parameters to be $Q = -0.43\% \pm 0.27\%$ and $U = 0.94\% \pm 0.27\%$ corresponding to $P = 1.03\% \pm 0.27\%$. In addition, it is possible to obtain measurements for two stars found in the ALFOSC field of view shown in Figure 6 (left). Both stars are bright, isolated targets, and based on the astrometric solutions from Gaia Data Release 3 (Gaia Collaboration et al. 2022) they also lie 150 pc above the Milky Way plane and should therefore be sufficiently far to probe the Milky Way dust content (Tran 1995). As such, they should be reliable estimators of the Galactic interstellar polarization (ISP). The SN is clearly offset from the stars on the *Q*–*U* plane (Figure 6), which is an indication of intrinsic polarization. Assuming the Galactic ISP can be obtained by averaging the two stars, we find Galactic ISP-corrected values for SN 2023emq of $Q = -0.24\% \pm 0.30\%$ and $U = 0.37\% \pm 0.30\%$, resulting in $P = 0.55\% \pm 0.30\%$ (corrected for polarization bias following Plaszczynski et al. 2014).

While we have no means to directly probe the host-galaxy ISP, its maximum value should correlate with the host extinction following $P_{ISP} < 9 \times E_{B-V}$ (Serkowski et al. 1975). Using the derived limit on host extinction ($E_{B-V} \lesssim 0.02$) we

find that the effect of host-galaxy dust content should be $P_{ISP,Host} \lesssim 0.19\%$. As the derived polarization degree ($P \sim 0.55\%$) is more significant, it is likely intrinsic to the SN. Given the spectrum at the time does not exhibit strong absorption lines that could induce polarization (e.g., Wang & Wheeler 2008), the polarization is likely that of the continuum. If the photosphere is an oblate ellipsoid, $P \sim 0.55\%$ corresponds to a physical minor over major axial ratio of $b/a \lesssim 0.9$ (Höflich 1991), but as shown by Pursiainen et al. (2022) the CSM can also be found in a disk/torus, and the CSM does not need to be in a uniform ellipsoidal shape. However, given the detection is not very strong, we conclude that the CSM shows a high degree of spherical symmetry, in perhaps marginally aspherical configuration.

Polarimetry of Type Ibn/Icn SNe is very scarce in the literature, and polarimetric data that probe the intrinsic properties of the SNe have been presented only for one Type Ibn and one Type Icn SN. The spectral polarimetry obtained for Type Ibn SN 2015G 5 days after discovery showed $P \sim 2.7\%$, indicative of high asymmetry (Shivvers et al. 2017), while the one epoch for Type Icn SN 2021csp at +3.5 days shows low polarization, implying high spherical symmetry (Perley et al. 2022). Additionally, Shivvers et al. (2016) presented three epochs of spectropolarimetry of the highly reddened Type Ibn SN 2015U at $\sim$+5 days and conclude that the observed polarization signal was dominated by the contribution of dust in the host galaxy, and no firm conclusions on the polarization of the SN were made. As such, our broadband polarimetry for SN 2023emq is only the third observation that constrains the photospheric geometry of Type Ibn/Icn SNe. The H-poor CSM appears to often show a high degree of spherical symmetry, but more events need to be observed to investigate the distribution of their photospheric shape.

4. Conclusions

We have presented an analysis of the photometric, spectroscopic, and polarimetric properties of the fast-evolving H-poor interacting SN 2023emq. While the rise of the SN is not particularly fast in the context of Type Ibn and Icn SNe, its initial decline ($\sim$0.20 mag day^{-1}) is remarkable and even comparable to AT 2018cow. After +20 days the decline rate slowed significantly to ($\sim$0.07 mag day^{-1}). Such a large transition in the decline rate is extreme and to our knowledge has not been seen before in interacting H-poor SNe. We modeled the bolometric light curve with a combined CSM interaction and nickel decay model and find good matches with $M_{\mathrm{ejecta}} \sim 0.32 M_{\odot}$ and $M_{\mathrm{CSM}} \sim 0.12 M_{\odot}$, with $\sim$0.006$M_{\odot}$ of ^{56}Ni. While the late-time light curve is still faster than expected of ^{56}Co to ^{56}Fe decay, it is likely that the radioactive decay is playing a part.

The SN was initially classified as Type Icn based on the prominent emission features at 4650 and 5700 Å identified as C III as typical in Type Icn SNe (e.g., Gal-Yam et al. 2022; Perley et al. 2022), but by +8 days the SN had evolved into a typical Type Ibn characterized by prominent, narrow He I emission features, possibly implying a transitional nature. We, however, conclude that SN 2023emq is a flash-ionized Type Ibn SN instead. As emission at 4650 and 5700 Å has been seen in a few Type Ibn SNe, just the presence of emission is not yet enough to classify the SN as Type Icn. The emission at 4650 Å seen in the first spectrum of SN 2023emq is dominated by He II with contribution from C III/N III, indicative of Type Ibn nature. Additionally, the C III λ4650 has typically a prominent P Cygni profile in Type Icn SNe, but only emission is present in SN 2023emq. However, while emission at 5700 Å has been reported in some Type Ibn SNe, it is remarkably strong in SN 2023emq and in this regard the SN is more similar to Type Icn SNe. In conclusion, based on our analysis we consider SN 2023emq a flash-ionized Type Ibn SN, but the strong emission at 5700 Å could indicate that the SN is between the Type Ibn and Icn populations if it is related to C III. More spectra obtained immediately after discovery are needed to investigate the importance of the emission at 5700 Å and further investigate the diversity of the flash-ionized features in core-collapse SNe.

We also obtained V-band polarimetry for SN 2023emq, making it only the third Type Ibn/Icn SN with optical polarimetry that probed the intrinsic emission from the SN. We find polarization degree $P = 0.55\% \pm 0.30\%$ after correction for Galactic ISP and polarization bias. Based on the upper limit on host extinction, the polarization is likely not caused by the host dust content, and we conclude that the polarization is intrinsic to the SN. Given the spectrum is dominated by interaction lines at the time, the result implies that the CSM shows high spherical symmetry in possibly marginally aspherical configuration. More polarimetric observations of these SN classes are required to characterize their geometric diversity and thus gain crucial insight to how the CSM is produced.

Appendix A
Bolometric Light Curve

The bolometric light curve of SN 2023emq was constructed using blackbody fits to the multiband epochs. The five epochs with UVOT data at +3–8 days and the NOT *BVRI* epoch at +20 days were fit with a blackbody model to determine the evolution of temperature and radius shown in Figure 7. For these six epochs, we generated the bolometric luminosity assuming the spectral energy distribution is described by the blackbody fits. During the rise with only *o*-band data, we used the linearly declining temperature curve to estimate the temperature at the time of each data point and estimated the bolometric luminosity by scaling the resulting blackbody to the *o*-band magnitude. We also tested the assumption of constant temperature during the rise by adopting the temperature measured at +3 days, but the bolometric light curve did not change significantly due to the small change in the temperature. After +20 days, we adopted the temperature found at +20 days (∼7500 K) and scaled the blackbody to the late-time *R*-band data. As such, our bolometric luminosity is well constrained only between +3 and +20 days. Outside this range the bolometric luminosities are uncertain and we have assumed 25% errors.
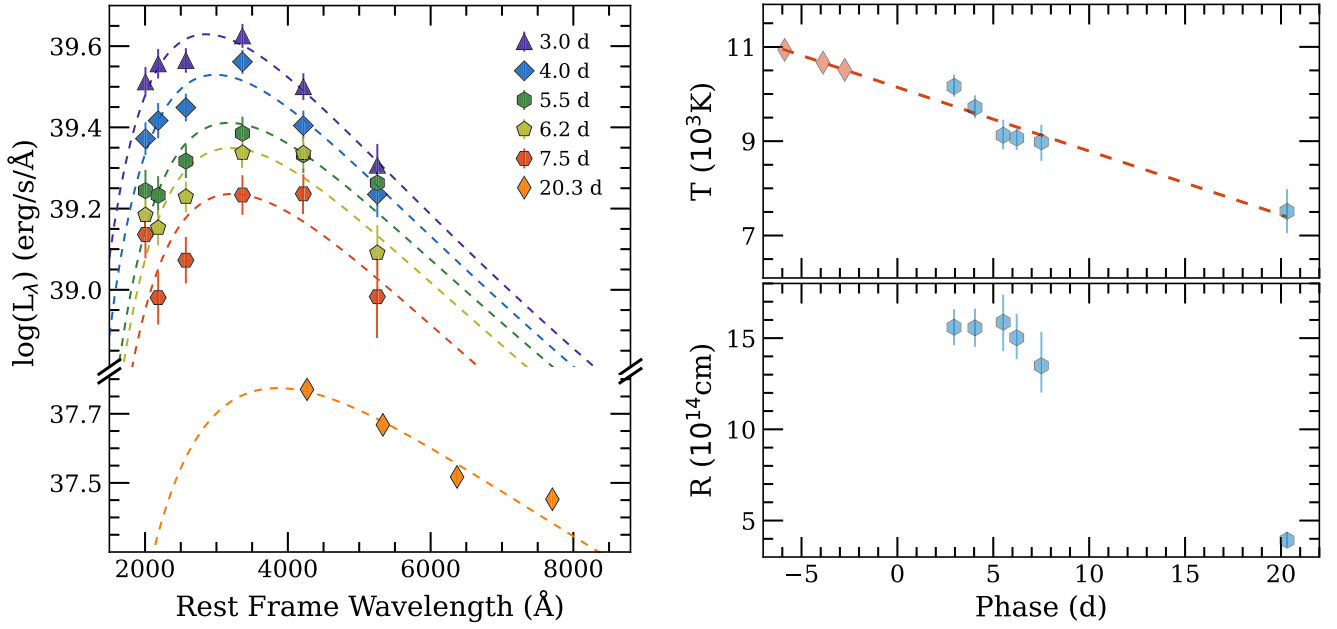
Figure 7. The blackbody modeling of SN 2023emq. Left: the blackbody fits to the six multiband epochs. Note the break on the *y*-axis. Right: the temperature and radius evolution of SN 2023emq derived from blackbody fits hexagons. The temperature is linearly declining, and the slope was used to determine the temperature at the time of *o*-band data points on the rise (diamonds).

Appendix B
Tables

In Table 1 we provide the photometry of SN 2023emq presented in this paper, and in Table 2 we provide the details of the spectroscopic time series.

Table 1
Photometry of SN 2023emq

Filter	MJD	Phase (days)	Mag	Error	Telescope
o	60031.2	−8.5	>20.41	⋯	ATLAS
r	60032.3	−7.4	>19.61	⋯	ZTF
o	60033.9	−5.9	19.11	0.14	ATLAS
o	60036.0	−3.9	17.68	0.03	ATLAS
o	60037.2	−2.7	17.25	0.04	ATLAS
UVW2	60043.1	3.0	18.32	0.09	Swift
UVM2	60043.1	3.0	18.02	0.09	Swift
UVW1	60043.1	3.0	17.65	0.08	Swift
U	60043.1	3.0	16.91	0.07	Swift
B	60043.1	3.0	16.73	0.08	Swift
V	60043.1	3.0	16.74	0.13	Swift
r	60043.4	3.3	17.44	0.06	ZTF

Note. The magnitudes are corrected for Galactic extinction. NOT/ALFOSC and VLT/FORS2 data are host-subtracted using the last epoch of VLT/FORS2 as template for *R* band and Legacy Survey data in the *g*, *r*, and *i* bands (Dey et al. 2019) for *B*, *V*, and *I* data, respectively.

(This table is available in its entirety in machine-readable form.)

Table 2
Spectroscopic Time Series of SN 2023emq

Date	MJD	Phase (days)	Telescope	Instrument	Grism/Arm	R (λ/Δλ)	Range
2023-04-03	60038.6	−1.3	FTS	FLOYDS-S	⋯	400/700	3500–10000
2023-04-14	60048.0	8.0	NOT	ALFOSC	Gr#4	360	3200–9600
2023-04-18	60052.1	11.6	NTT	EFOSC2	Gr#11/Gr#16	390/595	3380–10320
2023-04-28	60062.0	21.4	VLT	X-Shooter	UVB/VIS/NIR	5400/8900/5600	3000–24800

Note. The first spectrum is the classification one, publicly available in WISeREP.

ORCID iDs

M. Pursiainen https://orcid.org/0000-0003-4663-4300
G. Leloudas https://orcid.org/0000-0002-8597-0756
S. Schulze https://orcid.org/0000-0001-6797-1889
P. Charalampopoulos https://orcid.org/0000-0002-0326-6715
C. R. Angus https://orcid.org/0000-0002-4269-7999
J. P. Anderson https://orcid.org/0000-0003-0227-3451
F. Bauer https://orcid.org/0000-0002-8686-8737
T.-W. Chen https://orcid.org/0000-0002-1066-6098
L. Galbany https://orcid.org/0000-0002-1296-6887
M. Gromadzki https://orcid.org/0000-0002-1650-1518
C. P. Gutiérrez https://orcid.org/0000-0003-2375-2064
C. Inserra https://orcid.org/0000-0002-3968-4409
J. Lyman https://orcid.org/0000-0002-3464-0642
T. E. Müller-Bravo https://orcid.org/0000-0003-3939-7167
M. Nicholl https://orcid.org/0000-0002-2555-3192
S. J. Smartt https://orcid.org/0000-0002-8229-1731
L. Tartaglia https://orcid.org/0000-0003-3433-1492
P. Wiseman https://orcid.org/0000-0002-3073-1512
D. R. Young https://orcid.org/0000-0002-1229-2499

References

Appenzeller, I., Fricke, K., Fürtig, W., et al. 1998, Msngr, 94, 1
Astropy Collaboration, Price-Whelan, A. M., Sipőcz, B. M., et al. 2018, AJ, 156, 123
Astropy Collaboration, Robitaille, T. P., Tollerud, E. J., et al. 2013, A&A, 558, A33
Becker, A., 2015, HOTPANTS: High Order Transform of PSF ANd Template Subtraction, Astrophysics Source Code Library, ascl:1504.004
Bellm, E. C., Kulkarni, S. R., Barlow, T., et al. 2019, PASP, 131, 068003
Bertin, E., & Arnouts, S. 1996, A&AS, 117, 393
Bruch, R. J., Gal-Yam, A., Schulze, S., et al. 2021, ApJ, 912, 46
Bruch, R. J., Gal-Yam, A., Yaron, O., et al. 2023, ApJ, 952, 119
Charalampopoulos, P., Pursiainen, M., Leloudas, G., et al. 2023, A&A, 673, A95
Chatzopoulos, E., Craig Wheeler, J., & Vinko, J. 2012, ApJ, 746, 121
Chatzopoulos, E., Wheeler, J. C., Vinko, J., Horvath, Z. L., & Nagy, A. 2013, ApJ, 773, 76
Davis, K. W., Taggart, K., Tinyanont, S., et al. 2023, MNRAS, 523, 2530
Dey, A., Schlegel, D. J., Lang, D., et al. 2019, AJ, 157, 168
Drout, M. R., Chornock, R., Soderberg, A. M., et al. 2014, ApJ, 794, 23
Fassia, A., Meikle, W. P., Chugai, N., et al. 2001, MNRAS, 325, 907
Flewelling, H. A., Magnier, E. A., Chambers, K. C., et al. 2020, ApJS, 251, 7
Foley, R. J., Smith, N., Ganeshalingam, M., et al. 2007, ApJL, 657, L105
Förster, F., Cabrera-Vives, G., Castillo-Navarrete, E., et al. 2021, AJ, 161, 242
Fraser, M., Stritzinger, M. D., Brennan, S. J., et al. 2021, arXiv:2108.07278
Gaia Collaboration, Vallenari, A., Brown, A., & Prusti, T. 2022, A&A, 674, A1
Gal-Yam, A., Arcavi, I., Ofek, E. O., et al. 2014, Natur, 509, 471
Gal-Yam, A., Bruch, R., Schulze, S., et al. 2022, Natur, 601, 201
Gangopadhyay, A., Misra, K., Hiramatsu, D., et al. 2019, ApJ, 889, 170
Gangopadhyay, A., Misra, K., Hosseinzadeh, G., et al. 2022, ApJ, 930, 127
Harris, C. R., Millman, K. J., van der Walt, S. J., et al. 2020, Natur, 585, 357
Ho, A. Y. Q., Perley, D. A., Gal-Yam, A., et al. 2023, ApJ, 949, 120
Ho, A. Y. Q., Perley, D. A., Kulkarni, S. R., et al. 2020, ApJ, 895, 49
Höflich, P. 1991, A&A, 246, 481
Hosseinzadeh, G., Arcavi, I., Valenti, S., et al. 2017, ApJ, 836, 158
Hunter, J. D. 2007, CSE, 9, 90
Inserra, C. 2019, NatAs, 3, 697
Khazov, D., Yaron, O., Gal-Yam, A., et al. 2016, ApJ, 818, 3
Lyman, J., 2021 Astrophysics Source Code Library, ascl:2103.003
Makarov, D., Prugniel, P., Terekhova, N., Courtois, H., & Vauglin, I. 2014, A&A, 570, A13
McCully, C., Crawford, S., Kovacs, G., et al. 2018, astropy/astroscrappy: v1.0.5 Zenodo, doi: 10.5281/zenodo.1482018
Nagao, T., Kuncarayakti, H., Maeda, K., et al. 2023, A&A, 673, A27
Newville, M., Ingargiola, A., Stensitzki, T., & Allen, D. B. 2014, lmfit/lmfit-py, v1.2.2 Zenodo, doi:10.5281/zenodo.598352
Pastorello, A., Benetti, S., Brown, P. J., et al. 2015a, MNRAS, 449, 1921
Pastorello, A., Mattila, S., Zampieri, L., et al. 2008, MNRAS, 389, 113
Pastorello, A., Tartaglia, L., Elias-Rosa, N., et al. 2015b, MNRAS, 454, 4293
Pastorello, A., Wang, X. F., Ciabattari, F., et al. 2016, MNRAS, 456, 853
Pellegrino, C., Gonzalez, E. P., Farah, J., et al. 2023, TNSAN, 75, 1
Pellegrino, C., Howell, D. A., Terreran, G., et al. 2022a, ApJ, 938, 73
Pellegrino, C., Howell, D. A., Vinkó, J., et al. 2022b, ApJ, 926, 125
Perley, D. A., Ho, A. Y. Q., Yao, Y., et al. 2021, MNRAS, 508, 5138
Perley, D. A., Mazzali, P. A., Yan, L., et al. 2019, MNRAS, 484, 1031
Perley, D. A., Sollerman, J., Schulze, S., et al. 2022, ApJ, 927, 180
Plaszczynski, S., Montier, L., Levrier, F., & Tristram, M. 2014, MNRAS, 439, 4048
Poznanski, D., Prochaska, J. X., & Bloom, J. S. 2012, MNRAS, 426, 1465
Prentice, S. J., Maguire, K., Smartt, S. J., et al. 2018, ApJL, 865, L3
Pursiainen, M., Childress, M., Smith, M., et al. 2018, MNRAS, 481, 894
Pursiainen, M., Gutiérrez, C. P., Wiseman, P., et al. 2020, MNRAS, 494, 5576
Pursiainen, M., & Leloudas, G. 2023, TNSAN, 88, 1
Pursiainen, M., Leloudas, G., Cikota, A., et al. 2023, A&A, 674, A81
Pursiainen, M., Leloudas, G., Paraskeva, E., et al. 2022, A&A, 666, A30
Reguitti, A., Pastorello, A., Pignata, G., et al. 2022, A&A, 662, L10
Schlafly, E. F., & Finkbeiner, D. P. 2011, ApJ, 737, 103
Selsing, J., Malesani, D., Goldoni, P., et al. 2019, A&A, 623, A92
Serkowski, K., Mathewson, D. L., & Ford, V. L. 1975, ApJ, 196, 261
Shingles, L., Smith, K. W., Young, D. R., et al. 2021, TNSAN, 7, 1
Shivvers, I., Zheng, W., Mauerhan, J., et al. 2016, MNRAS, 461, 3057
Shivvers, I., Zheng, W. K., Van Dyk, S. D., et al. 2017, MNRAS, 471, 4381
Smartt, S. J., Valenti, S., Fraser, M., et al. 2015, A&A, 579, A40
Smith, K. W., Smartt, S. J., Young, D. R., et al. 2020, PASP, 132, 085002
Smith, K. W., Williams, R. D., Young, D. R., et al. 2019, RNAAS, 3, 26
Tonry, J., Denneau, L., Weiland, H., et al. 2023, TNSTR, 2023-698, 1
Tonry, J. L., Denneau, L., Heinze, A. N., et al. 2018, PASP, 130, 064505
Tran, H. D. 1995, ApJ, 440, 565
Vernet, J., Dekker, H., D'Odorico, S., et al. 2011, A&A, 536, A105
Virtanen, P., Gommers, R., Oliphant, T. E., et al. 2020, NatMe, 17, 261
Wang, L., & Wheeler, J. C. 2008, ARA&A, 46, 433
Wiseman, P., Pursiainen, M., Childress, M., et al. 2020, MNRAS, 498, 2575
Yao, Y., Ho, A. Y. Q., Medvedev, P., et al. 2022, ApJ, 934, 104
Yaron, O., & Gal-Yam, A. 2012, PASP, 124, 668